RSC Advances

PAPER

Cite this: *RSC Adv.*, 2016, **6**, 100829

Carbon dioxide activation and transformation to HCOOH on metal clusters (M = Ni, Pd, Pt, Cu, Ag & Au) anchored on a polyaniline conducting polymer surface – an evaluation study by hybrid density functional theory†

Ramasamy Shanmugam,[ad] Arunachalam Thamaraichelvan,[b] Tharumeya Kuppusamy Ganesan[c] and Balasubramanian Viswanathan*[d]

Received 17th August 2016
Accepted 17th October 2016

DOI: 10.1039/c6ra20715d

www.rsc.org/advances

Developing new efficient catalysts for the electrochemical reduction of carbon dioxide to formic acid is important in the process of mitigating environmental CO_2. In the present work, we have designed metal (M) clusters anchored on a polyaniline (PANI) conducting polymer electrode (M@PANI), where, M = Ni, Pd, Pt, Cu, Ag & Au, and evaluated their potential catalytic activity towards CO_2 reduction by means of computational hydrogen electrode using hybrid density functional theory methods. The predicted binding energy and electronic properties of M@PANI suggest a thermodynamically feasible reaction which retains its conducting property with enhancement. The modified electrodes favour the formation of HCOOH involving H*COO species *via* the formate pathway. The computed limiting potentials suggest that Cu@PANI is a suitable electrode material for the CO_2 reduction reaction leading to HCOOH.

Introduction

In recent years, renewable energy sources have received immense attention due to their utility in the electrochemical conversion of greenhouse gas, CO_2, into value added chemicals[1–3] which can potentially decrease the environmental impact of CO_2. CO_2 can produce a variety of chemicals[4–7] among which HCOOH is considered in the present work. Being a highly functionalised molecule, the activated CO_2^- species has been used as a building block in fine chemical production,[8,9] fuel cells[10–12] and hydrogen storage.[13] General electro-reduction of CO_2 has been carried out on electrodes either in a direct or an indirect manner. Although a large number of electrode[14–20] materials have been tried in this regard, the low efficiency of the process needs to be improved. Special attention is required in the choice of electrode material for the production of chosen products from CO_2. HCOOH production is feasible on certain metal electrodes such as zinc, lead, mercury, thallium, indium, tin, cadmium and bismuth,[21,22] though it requires a high negative potential of about −2.0 V *vs.* SCE making the yield very low. Various electrode materials were attempted in improving the efficiency by decreasing the over potential.[23–26]

The main problem in electro reduction of CO_2 is the stability of chosen electrodes. Certain electrodes are not stable both in acidic and basic media. During the reaction, intermediate ions in the medium can change the pH. Hence, keeping the electrode for a prolonged period under stable condition is desirable. Growing interest in using polymer supported systems has been due to their enhanced activity in CO_2 transformation compared to unsupported one.[27–29] Polyaniline (PANI) as a conducting material has special characteristics which include easy synthesis, low cost and stability at ordinary conditions.[30] It plays a vital role in many potential applications[30] including light emitting diodes,[31] fuel cells,[32] capacitor,[33] super capacitor,[34] selective electrode,[35] electrical conductivity,[36] redox potential higher than metal, corrosion-resistance[37,38] tuneable solubility and thermal stability.[39]

Composites of PANI were used in electro based sensors,[40] as well as catalytic and photo catalytic reactions.[41,42] Recent reports reveal that a multifunctional catalyst exhibits better activity in CO_2 fixation reactions.[43,44] CO_2 reduction involves electron addition in the first step followed by addition of proton, and then a series of proton, electron and a couple of proton and electron. All these reaction steps are competitive and control the product formation and selectivity. Under these conditions, a suitable catalyst must change its role according to the nature of the substrate. However, this does not happen in the most

[a]*Department of Chemistry, Thiagarajar College, Madurai, Tamilnadu 625 009, India*
[b]*Faculty of Allied Health Sciences, Chettinad Hospital & Research Institute, Kelambakkam, Tamilnadu 603 103, India*
[c]*Department of Chemistry, The American College, Madurai, Tamilnadu 625 002, India*
[d]*National Center for Catalysis Research, Indian Institute of Technology Madras, Chennai, Tamilnadu 600 036, India. E-mail: bvnathan@iitm.ac.in*

† Electronic supplementary information (ESI) available. See DOI: 10.1039/c6ra20715d

routinely used catalytic systems. Therefore, designing a catalyst with multifunctional activity is desired. PANI can serve as a better candidate in such reactions, since it can either uptake or release electron and proton[45] by altering its structural form. In addition, it can provide a good support in stabilising the metal nanoparticles.[46] Sulfonated PANI has found application in CO_2 sensing.[47] Moreover, PANI is used in hydrogenation of N_2 and CO_2 under electrochemical conditions.[48,49] Metals like Ni, Pd, Pt, Cu, Ag, and Au serve an electrodes in most of the electro reduction reactions of CO_2.[50] Small quantities of metals are preferred due to their availability and cost. Generally, pure forms of Ni, Pd, Pt, Cu, Ag, and Au are not useful in the production of HCOOH due to CO positioning and their tendency to form other hydrogenated products.[21] However, suitably modified metal electrodes are performing better activity towards HCOOH formation with lower negative potentials.[12,22,23,26,51–53] Ni coated PANI has been used in sensors[54] and absorption of microwaves.[55] Pd–PANI/carbon nanotube composite has better catalytic activity towards conversion of CO_2 to HCOOH.[56] Platinum and its based alloys supported on PANI electrode were used in oxidation of glycerol.[46] Copper polypyrrole electrode was employed in CO_2 reduction under high pressure conditions.[57] PANI protected Ag behaves as a good electrode in oxidation of hydrazine.[58] Gold–PANI nanocomposite has performed better in electrochemical reduction of oxygen than other counterparts.[59] These reports reveal that metal@PANI systems have a significant role in electrode mediated reactions. Hence, designing and evaluating the activity of a suitable electrode with multiple functionality involving metal–PANI system for CO_2 reduction reaction is more trustworthy.

The present work aims to probe as catalyst, the electrodes made of metal clusters anchored on PANI as polymer support, towards CO_2 reduction leading to HCOOH by employing hybrid density functional theory methods.

Molecular models

The model used for the study was constructed as follows: (i) the structure of metal cluster with M_7 unit, where, M = Ni, Pd, Pt, Cu, Ag & Au studied extensively in literature,[60–65] was chosen. (ii) An oligomer of PANI, which consists of 3 units of aniline was used to mimic the polymeric site. (iii) Subsequently, the metal M_7 unit was placed on the terminal of oligomer at the N site and is referred to as M@PANI. This configuration was considered for further study.

Computational techniques

The geometry optimization of pure M@PANI and those with adsorbates were performed at B3LYP level of hybrid density functional theory using a basis set of LANL2DZ for metals and 6-31G* for other elements. Since, the configurations of M@PANI are present in the ground state, the total spin value of 1 for Ni, Pd & Pd and 2 for Cu, Ag & Au models were assigned respectively. Using the same level of theory, vibrational frequencies were calculated to identify whether the obtained configuration is either a stationary point or transition state on the potential energy surface. The binding energy of M@PANI clusters was obtained using the formula of $BE_M = E_{M@PANI} - E_M - E_{PANI}$ where, E_M, $E_{M@PANI}$, and E_{PANI} are total zero point energy (ZPE) corrected electronic energy of metal cluster, metal PANI and pure PANI respectively. For the adsorbates the binding energy was calculated by, $BE_{ads} = E_{adsorbate+M@PANI} - E_{M@PANI} - E_{adsorbate}$ where, $E_{Cu_{adsorbate+M@PANI}}$, $E_{M@PANI}$ and $E_{adsorbate}$ are zero point energy corrected electronic energy of $Cu_{adsorbate+M@PANI}$, M@PANI and adsorbate respectively. Ab initio molecular dynamics (AIMD) simulations were performed by using the final configurations obtained in the geometry optimisation as the initial structure. The ab initio Born–Oppenheimer molecular dynamics at B3LYP/LANL2DZ level was employed to find the stability of the electrode. Natural Bonding Orbital (NBO) analysis was carried out using NBO 3.1 (ref. 66) software implemented in Gaussian 09. Computational hydrogen electrode method[67–69] was applied to analyze the free energy of reaction pathway. For an elementary reaction, $A^* + (H^+ + e^-) \rightarrow AH^*$, the free energy is defined as, $\Delta G_{A^* \rightarrow AH^*}(U) = G_{AH^*} - G_{A^*} - 0.5G_{H_2} + n_e(U)$ where, the terms G, n_e and U represent free energy, number of electrons and an applied potential respectively. All these quantum mechanical calculations were carried out using Gaussian 09 software package.[70] Density of States (DOS) and Partial Density of States (PDOS) were plotted using GaussSum software.[71]

Results and discussion

Structural models designed for M–PANI

The metal cluster anchored on oligomer model of M–PANI, considered for the examination is depicted in Fig. 1. Studies on M_7 (M = Ni, Pd, Pt, Cu, Ag & Au) clusters are extensively available in literature.[60–65] The M_7 clusters anchored on oligomer containing three units of aniline are represented in Fig. 1a–f respectively.

The metal clusters were anchored through metal–nitrogen sigma bond. The structural parameters of M@PANI are presented in Table 1.

The observed bond distances of M–N reveal a slight variation compared to those observed in complexes.[72–75] This is attributed to the cluster nature of metal instead of being a single atom

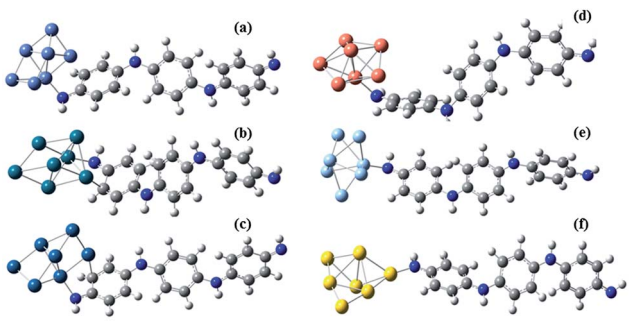

Fig. 1 Optimised geometries of M@PANI, where M is (a) Ni, (b) Pd, (c) Pt, (d) Cu, (e) Ag and (f) Au respectively.

Table 1 Binding energy (ΔE) eV, bond angle (θ)°, bond length (l) Å and bond order for M@PANI

		θ (°)	l (Å)		Bond order
M	ΔE (eV)	C–N–M	C–N	N–M	N–M
Ni	−2.25	108.71	1.37	1.86	0.745
Pd	−1.48	110.31	1.35	2.08	0.715
Pt	−3.83	110.96	1.34	2.03	0.674
Cu	−1.83	119.99	1.36	1.95	0.652
Ag	−1.07	121.02	1.38	2.16	0.739
Au	−1.72	131.26	1.34	2.11	0.478

which causes electronic and steric repulsion with the oligomer unit. Furthermore, the bond order of M–N experiences a gradual decrease from Ni to Au with the exception being Ag, where an increase in observed. Pure clusters of all metals have pentagonal bipyramid structure (ESI S1†). On anchoring, the geometry of metal clusters for Ni, Pd and Pt was found to become distorted cube. However, Cu and Ag exhibited pentagonal bipyramid geometry while Au revealed distorted pentagonal bipyramid geometry. This structural distortion reveals the strong interaction of the metal with the conducting polymer. The data for the angle, C–N–M are presented in Table

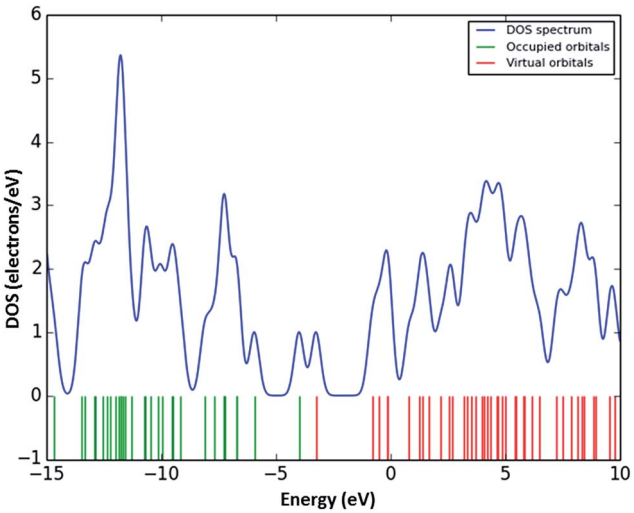

Fig. 3 Density of states of pure PANI.

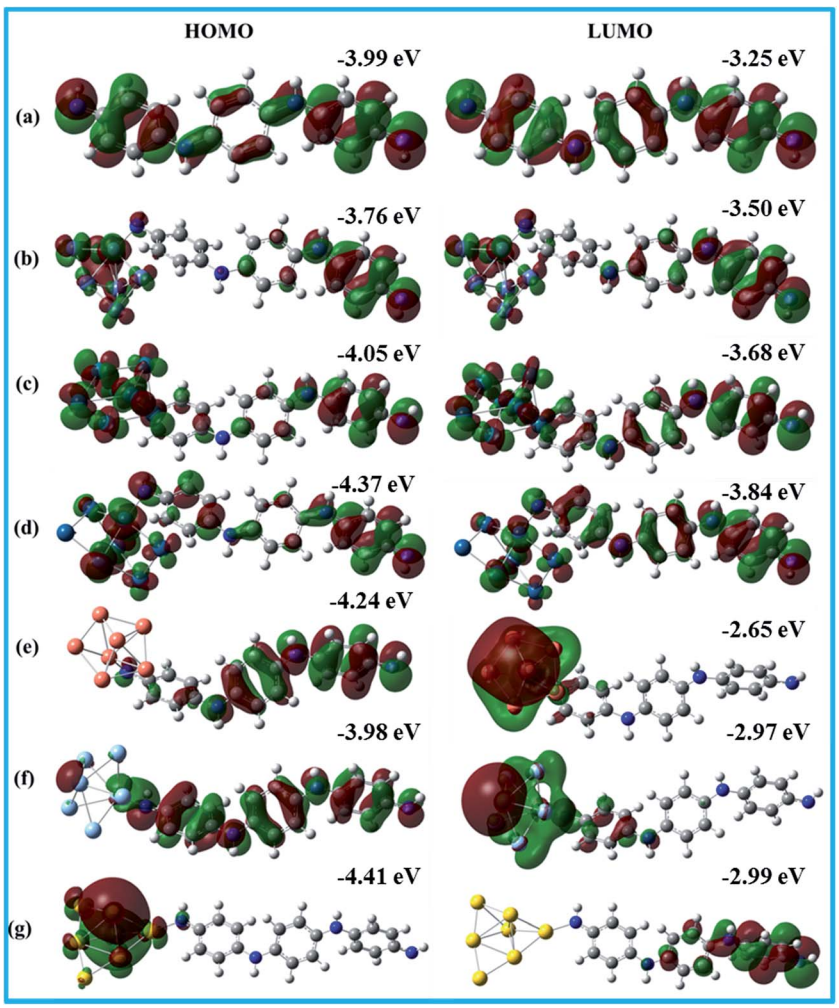

Fig. 2 Frontier molecular orbitals of (a) pure PANI and M@PANI where M is (b) Ni, (c) Pd, (d) Pt, (e) Cu, (f) Ag and (g) Au respectively with their energies.

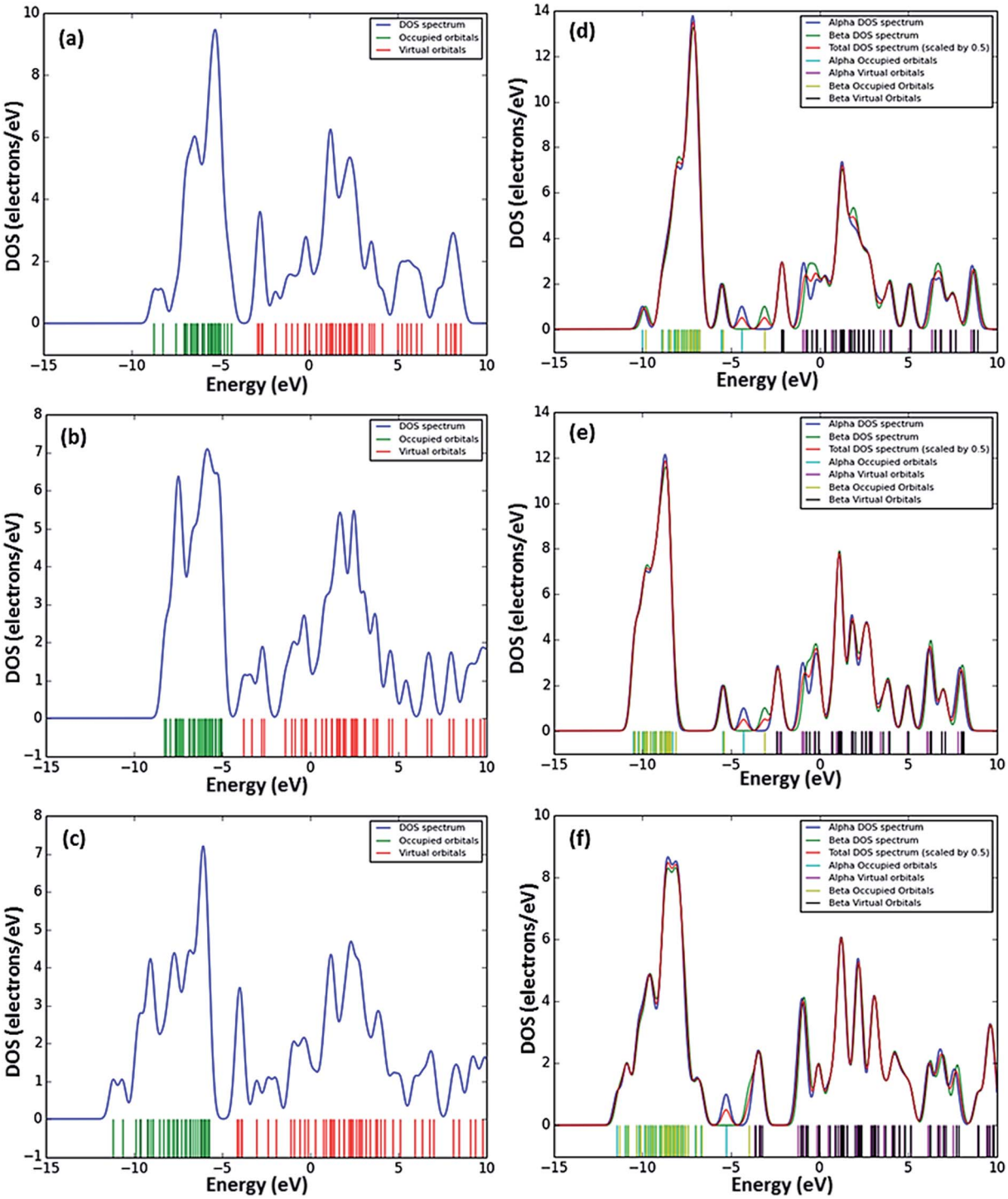

Fig. 4 PDOS of pure metal clusters (a) Ni, (b) Pd, (c) Pt, (d) Cu, (e) Ag and (f) Au.

1, reveal that the cluster is located approximately in a triangular fashion which is seen above the polymer plane. The binding energy between metal and PANI shows a negative value and predict that the anchoring of metal clusters on PANI is a thermodynamically feasible process. The order of binding energy for different metals is found to be Pt > Ni > Cu > Au > Pd > Ag. That all the computed infrared frequencies are positive, predicts that the configurations are at stationary points in the potential energy surface. Furthermore, the stability of metal–PANI is characterised by means of ab initio Born–Oppenheimer molecular dynamics (BOMD) method which is presented in ESI S2.†

Frontier molecular orbital (FMO) and electronic structure analysis

The conducting nature of PANI is mainly controlled by its orbital energy density of HOMO and LUMO and the position

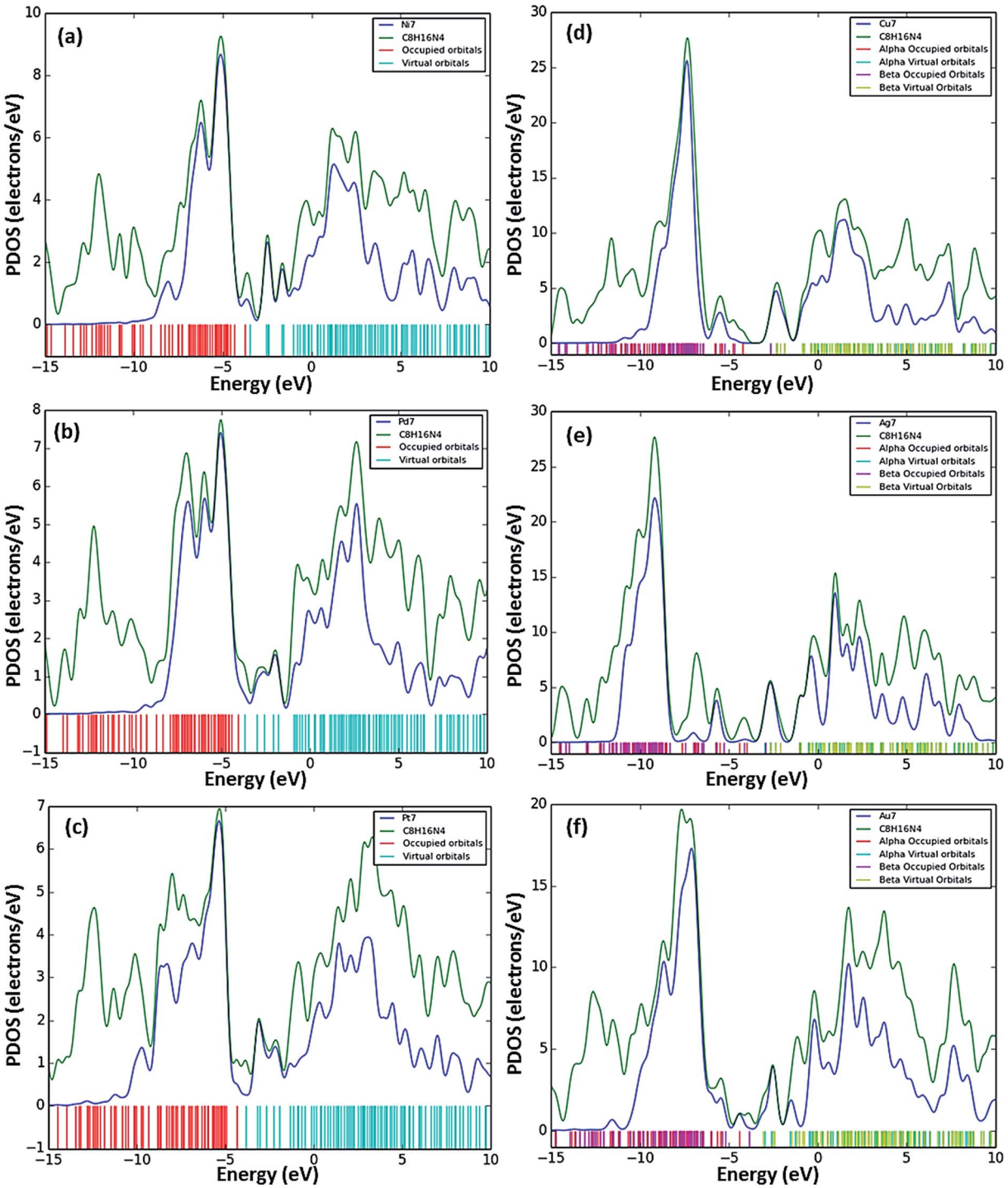

Fig. 5 Partial density of states of M@PANI where M is (a) Ni, (b) Pd, (c) Pt, (d) Cu, (e) Ag and (f) Au respectively.

where it is located. While anchoring of metal cluster on PANI may perturb the frontier molecular orbitals of PANI, it helps to locate at specific sites on M@PANI and control of electron transfer processes. Frontier molecular orbital (HOMO and LUMO) contours of pure and M@PANI are depicted in Fig. 2.

The HOMO and LUMO of pure PANI spread over π bond between C–H and nitrogen, in a symmetric manner. The FMO analysis of M@PANI reveals that, anchoring of metal cluster shifted the HOMO and LUMO orbitals. In Ni, Pd and Pt, the HOMO comprises of orbitals located on metal, the π-CH and nitrogen. Compared to pure PANI, the shift of HOMO was observed in the π-CH which is present adjacent to the metal cluster. The same trend was observed in LUMO also. It is interesting to note that the shift was not similar in Pt and Pd. While the HOMO is distributed all the metal atoms in the cluster, in Pd, it is concentrated on the metal atoms nearer to

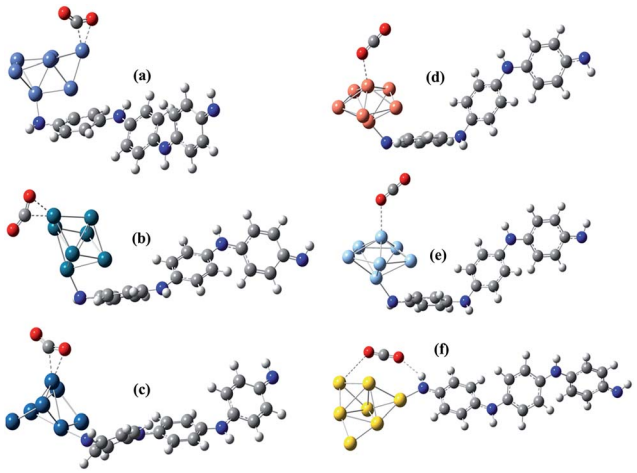

Fig. 6 Geometry optimized configurations of CO_2 on M@PANI where M is (a) Ni, (b) Pd, (c) Pt, (d) Cu, (e) Ag and (f) Au respectively.

the aniline molecule of PANI in Pt. In Pt and Pd, the orbitals observed are denser than in Ni and are as dense as in pure PANI. In contrast to this, the HOMO in Cu@PANI is mostly on PANI and LUMO is centred on Cu. On moving to Ag system, the HOMO levels gradually increase their presence on Ag and the LUMO moves gradually towards PANI. On Au, the HOMO was completely shifted to metal site and the LUMO was located on PANI's site. The participation of metal orbitals in the HOMO population is in the order, Pd > Pt > Ni > Au > Ag > Cu. The order appears to be influenced by the valency and size factors of the metals. While higher valence state leads to greater electron population of HOMO, the atom with larger size contributes more among a given group of elements. The perturbation of HOMO and LUMO is due to the electron releasing nature of the metal which is influenced by the arrangement of atoms in the clusters.

In general, individual metal and PANI reveal conducting behaviour. Anchoring of metal on PANI alters the conducting property of the polymer. It is essential to know the electronic properties of M@PANI in a detailed manner for better understanding of its conducting properties. Density of states of pure PANI, pure metal clusters and M@PANI are presented in Fig. 3–5 respectively. The values corresponding to HOMO and LUMO are presented in Fig. 2. In pure PANI (Fig. 3), the DOS is made up of s and p orbitals. The HOMO and LUMO contours in PANI reveal that in Ni, Pd & Pt catalyst same atom contributes to both the HOMO and LUMO. However, in Cu, Ag & Au, the HOMO & LUMO are centred in different regions. Hence, the HOMO and LUMO overlap with a minimum gap leading to metal like conducting behaviour of PANI.[76] Typically, metals are good conductors, though the conducting property may change at nano level. The PDOS of pure metal clusters (Fig. 4) suggests that the metallic behaviour may be due to the population of mainly d orbital rather than s and p orbitals. Further, the orbitals in PANI are overlapping with valance and conduction bands of metal clusters from (a) to (f) (Fig. 5). PDOS of M@PANI reveals that there is no energy gap window upon anchoring of metal on PANI near HOMO–LUMO region. This result suggests that the M@PANI still retains it conducting behaviour. Since the energy gap between HOMO and LUMO is inversely proportional to the reactivity of the material, the order of any reaction that depends redox property may be in the order Cu > Au > Ag > Pt > Pd > Ni.

Adsorption of CO_2 on PANI

M@PANI is in a heterogeneous environment consisting of a polymer and metal cluster unit, the interaction of CO_2 with polyaniline site has been predicted to be predominately physical adsorption.[77] Hence, the interaction of CO_2 at PANI site was not taken into account and the metal site alone was considered for CO_2 interaction. Such an interaction may be through various coordination modes through carbon, oxygen and combined forms are possible.[78] Among the different modes, the metal–carbon bond *via* CO_2 bent mode was considered for activation of CO_2. The configurations of CO_2 interaction with M@PANI for different M atoms after energy minimisation are presented in Fig. 6. The binding energy and structural parameters for the above interactions are presented in Table 2.

Data on binding energy reveal that except for copper, all other clusters weakly hold CO_2 on their surfaces. On the other hand, the structural features of adsorbed CO_2 on Cu@PANI resemble that of pure CO_2 though the binding energy reveal that CO_2 is adsorbed through chemisorption mode. A similar trend is observed in Pd and Pt too. However Ni, Pd and Pt clusters remarkably play a vital role in altering the bond angle of CO_2. As seen in the table, the angle of CO_2 is decreased from 180° to about 34.93°, 28.78° and 33.18° on Ni, Pd and Pt clusters

Table 2 The calculated adsorption energies (E_{ads}, eV), structural parameters and NBO charge ($|q|$) of CO_2 on M@PANI

		Angle (°)	Bond order		Bond length (Å)					$\|q\|$		
	E_{ads}	O–C–O	C–O	C–O	C–O	C–O	C–N	M–N	M–N–C	C	O	O
CO_2		180	2.000	2.000	1.16	1.16						
Ni	−0.70	145.07	1.728	1.437	1.20	1.25	1.37	1.85	106.80	0.798	−0.555	−0.588
Pd	−0.20	151.22	1.577	1.823	1.22	1.19	1.35	2.07	110.08	0.848	−0.567	−0.535
Pt	−0.27	146.82	1.437	1.840	1.25	1.19	1.34	2.04	111.09	0.469	−0.356	−0.358
Cu	−1.23	179.54	1.816	2.031	1.17	1.16	1.36	1.95	118.95	1.082	−0.514	−0.478
Ag	−0.19	179.78	1.867	2.037	1.17	1.16	1.35	2.18	120.76	1.072	−0.523	−0.488
Au	−0.06	178.87	1.942	1.981	1.17	1.16	1.34	2.11	131.67	1.067	−0.537	−0.499

Table 3 Calculated vibrational frequencies of CO_2 on M@PANI (cm^{-1})

O–C–O asymm stretching	C–O symm stretching
1927	1186
2057	1225
2009	1187
2424	1364
2425	1367
2429	1371

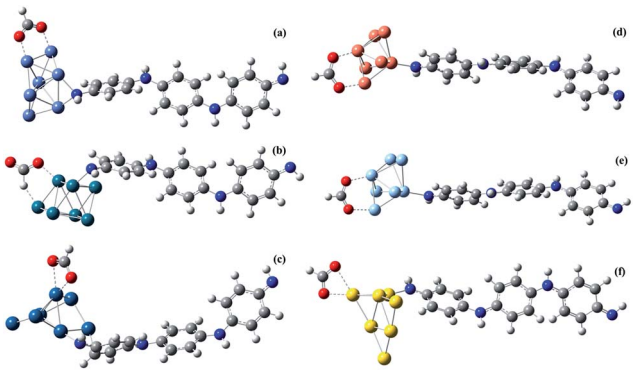

Fig. 7 Geometry optimized configuration of HCOO on M@PANI where, M in (a) Ni, (b) Pd, (c) Pt, (d) Cu, (e) Ag and (f) Au respectively.

respectively. The NBO charge analysis indicates that two types of charge transfer take place, the first being from metal onto CO_2 with values of, $-0.345q$, $-0.254q$ and $-0.245q$ on Ni, Pd and Pt respectively in the M@PANI. The second type of electron transfer from CO_2 to M where, a positive charge is observed on CO_2 due the weaker adsorption. The corresponding charges are Cu($0.09q$), Ag($0.061q$) and Au($0.031q$) on M@PANI. The negative charge transferred from M@PANI to CO_2 alters its bond angle leading to structural changes. Similar structural changes are observed in pure metal clusters also. The angles for O–C–O bond found in Pd and Ni are smaller than those in other M@PANI and for Ni, it is 6.15° lower than those for Pd and Pt indicating that in Ni, the metal–polymer support interaction predominates. Thus, the polymer support helps only to stabilise the cluster in the new geometry rather than in free form geometry. In general, during the interaction, the adsorbate will be able to change the geometry of the adsorbent. The calculated values of M–N bond length and M–N–C angle for the different metals after interaction are presented in Table 2. The values resemble those observed in pure M@PANI indicating that, even after interaction with adsorbate, the configuration of the adsorbent was not changed. Thus, the M@PANI system is stable under the reaction conditions. All the computed frequencies of CO_2 adsorbed on M@PANI are positive revealing that the configurations are on the stationary points in the potential energy surface. Selected vibrations of CO_2 are presented in Table 3.

Adsorption of HCOO* species on M@PANI

Subsequent to the interaction of CO_2 with M@PANI, a proton and an electron in the medium attach to the species to produce either formate (H*COO) or *COOH species leading to two pathways for HCOOH formation. The further stability of the species is controlled by the strength of adsorption strength thus

Table 4 The calculated adsorption energies (E_{ads}, eV) and structural parameters of HCOO* and COOH* species on M@PANI

M	E_{ads}		Angle (°)	Bond length (Å)					
	HCOO	COOH	O–C–O	C–H	C–O	C–O	C–N	M–N	M–N–C
CHOO			113.15	1.10	1.25	1.25	—	—	—
Ni	−9.13	−7.13	127.10	1.10	1.26	1.26	1.41	1.98	121.49
Pd	−3.09	−3.15	131.08	1.18	1.21	1.28	1.35	2.05	111.00
Pt	−3.23	−2.71	121.42	1.09	1.25	1.28	1.33	2.06	111.74
Cu	−2.99	−1.23	128.52	1.10	1.26	1.26	1.33	1.96	133.86
Ag	−2.61	−1.14	129.94	1.10	1.26	1.26	2.23	1.33	133.37
Au	−2.61	−2.14	124.63	1.10	1.27	1.25	1.33	2.08	128.65

Table 5 Calculated vibrational frequencies of HCOO on M@PANI (cm^{-1})

M	C–H out of plane bending	C–O symm str.	C–O asymm str.	O–C–O scissor	C–H in plane bending	C–H stretching
Ni	1053	1389	1631	766	1407	3061
Pd	946	1195	1820	763	1328	2057
Pt	1037	1387	1615	798	1324	3076
Cu	1047	1374	1630	767	1408	3018
Ag	1048	1367	1640	756	1412	2961
Au	1047	1380	1634	795	1343	3012

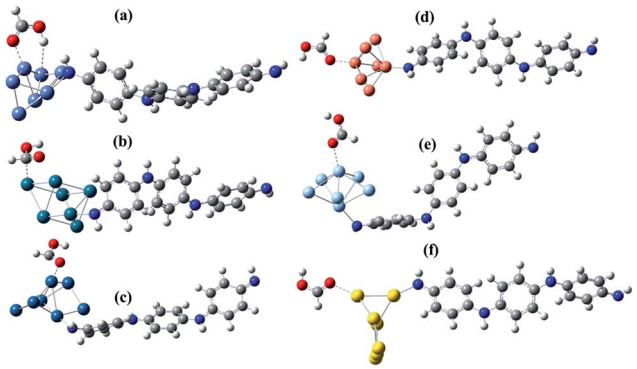

Fig. 8 Geometry optimized configuration of HCOOH on M@PANI where M is (a) Ni, (b) Pd, (c) Pt, (d) Cu, (e) Ag and (f) Au respectively.

making available the species for the reaction. The optimised geometries of the formate on M@PANI site are shown in Fig. 7. The binding energy and structural features of the optimised HCOO on M@PANI are given in Table 4. The values for H*COO and *COOH are negative indicating the thermodynamic feasibility of formation of both the species. The fact that the H*COO species has greater binding energy than *COOH reveals that H*COO species is preferably adsorbed compared to *COO and cover the active site predominantly to enter into further reaction.

The formate species is adsorbed mainly through two oxygen atoms *via* the bridge bidendate mode. However, in Pd, the HCOO is held *via* bridge bidendate mode not by two oxygen atoms but connected *via* H–Pd on one side and through O–Pd on the other side with a distance of 1.93 Å and 2.08 Å respectively. It is interesting to observe this bridge on Ni, Cu and Ag with two metal atoms, while in Pt and Au, single metal site forms the bridge with both oxygens. The bond length of C–H and C–O are more or less similar to those observed in free HCOO species. The data indicate that the two C–O bonds in HCOO exhibit double bond character. Alteration of bond length in the symmetric one requires more energy than that for the asymmetric one. Hence, there is not much change observed in C–O bond. The angle at carbon of O–C–O was greatly influenced, which is attributed to the formation of bridge for the adjustment of coordination between the two metal atoms which are located at a distance greater than that of O–O distance in HCOO. During the interaction, the structural features of interface between the metal and PANI are slightly modified. This reveals that the interface facilitates the interaction with adsorbate in a flexible manner. To verify whether this mode of adsorption of formate is in the stationary point, the vibrational frequencies were calculated. All the values, except for Au, are positive which indicate that except Au, all are located on stationary points and Au is present in the transition state. The characteristic vibrations for the CHOO obtained from the computations are presented in Table 5. The frequency data reveal that there is a small difference among the values of vibrational modes of various M@PANI systems which is metal dependant.

Table 6 The calculated adsorption energies (E_{ads}, eV) and structural parameters of HCOOH* on M@PANI

		Bond length (Å)							Angle (°)	
M	E_{ads}	M–H*COOH	C–H	O–H	C═O	C–O	C–N	M–N	M–N–C	O–C–O
Ni	−1.38	1.92	1.09	0.97	1.27	1.33	1.37	1.88	91.53	123.05
Pd	−0.54	2.16	1.10	0.97	1.27	1.38	1.35	2.07	111.51	120.06
Pt	−0.58	2.19	1.09	0.97	1.27	1.35	1.34	2.04	111.23	121.87
Cu	−0.39	2.09	1.09	0.98	1.22	1.32	1.36	1.89	130.44	123.84
Ag	−0.46	2.44	1.09	0.98	1.21	1.32	1.36	2.19	118.55	124.23
Au	−0.76	2.37	1.09	0.97	1.22	1.32	1.37	2.02	129.81	123.72

Table 7 Calculated vibrational frequencies of HCOOH on M@PANI (cm^{-1})

M	C–H out of plane bending	C═O str.	O–H str.	C–H str.	C–H + OH in plane bending	C–OH str.	O–H out of plane bending	C–H in plane bending
Ni	867	1554	3670	3149	1299	1096	529	1354
Pd	892	1493	3676	2971	1260	1059	532	1313
Pt	930	1550	3670	3130	1313	1113	547	1347

M	C–H out of plane bending	C═O str.	O–H str.	C–H str.	C–H + OH in plane bending	OH in plane bending	O–H out of plane bending	C–H in plane bending
Cu	1066	1778	3649	3152	1194	1361	721	1408
Ag	1065	1792	3652	3137	1186	1351	720	1416
Au	1066	1769	3646	3155	1194	1361	723	1412

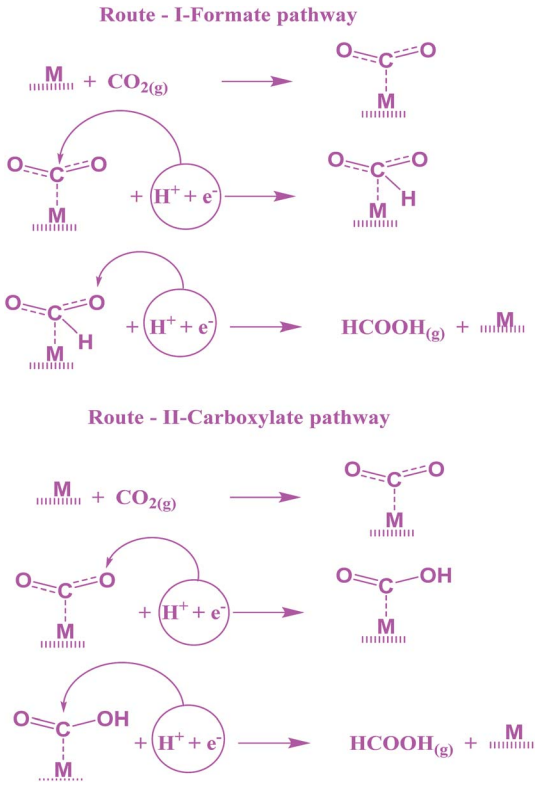

Fig. 9 Schematic representation of electrochemical reduction of CO_2 *via* different reaction pathways to formic acid.

Adsorption of HCOOH on M@PANI site

For the elucidation of the most stable adsorption site for HCOOH on M@PANI, HCOOH was placed on metal and allowed for full relaxation. The final configurations obtained are depicted in Fig. 8. HCOOH on M@PANI (M = Ni, Pd & Pt) is independently located. On Ni, HCOOH is coordinating *via* bidendate mode through O and H of C=O and O–H respectively with two adjacent metal atoms. However, monodentate coordination of HCOOH is observed on Pd through C. In the case of Pt, only a monodentate coordination was observed through O of C=O to the metal. In contrast to the above, HCOOH is held on Cu, Ag and Au through monodentate coordination from O of C=O perpendicular to the metal cluster. The distance between the HCOOH and M reveals that instead of a typical bonding, a weak interaction operates and hold the molecule onto the metal site. The binding energy and structural features of M@PANI are given in Table 6. That the HCOOH has a tendency to get adsorbed spontaneously on the metal site is revealed by the data. Ni@PANI has the maximum binding energy compared to other M@PANI systems. On adsorption, the M–N and C–N distances remains constant and are comparable to the values in pure form which indicates that the structure is stable. The stability of the cluster was further evaluated by means of frequency calculation. All the vibrational frequencies returned positive values thus predicting that the resultant configuration is present in one of the energy minima in the potential energy profile. Furthermore, selected vibrations related to HCOOH are tabulated in Table 7. The frequencies for Ni, Pd and Pt return lower frequencies than those of Cu, Ag and Au systems.

Electrochemical reduction of CO_2 to HCOOH

The electrochemical transformation pathway of CO_2 to HCOOH proceeds through the following steps:[53] (i) the gaseous CO_2 is coupled with an electron available in solution to form CO_2^- species, which is further adsorbed on the metal site. Subsequently, the reaction proceeds *via* two possible path ways: (ii-a) since the surface species has negative charge on O, the available

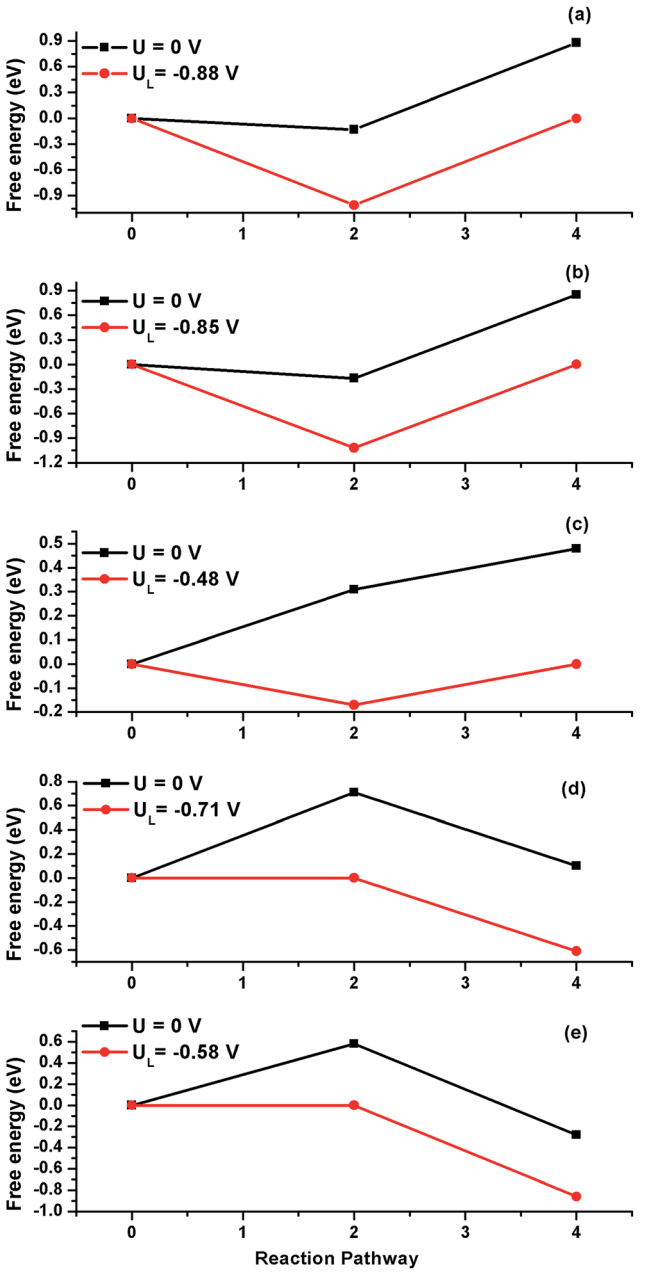

Fig. 10 Calculated Gibbs free energy profile without (U-black lines), and with applied potential (U_L-red lines) for CO_2 electroreduction to HCOOH through formate pathway on M@PANI where M = (a) Pd, (b) Pt, (c) Cu, (d) Ag, and (e) Au.

proton in solution reacts to form COOH* species in the adsorbed state (carboxylate pathway). (ii-b) Contrary to (ii-a), $H^+ + e^-$ in the solution attack the carbon of CO_2^- to form adsorbed $HCOO^-$ species (formate pathway). (iii) Further addition of a $H^+ + e^-$ couple to COOH or $HCOO^-$ leads to HCOOH finally. The above scheme is presented in Fig. 9. As seen from the binding energy data, Ni@PANI exhibits greater binding energy than other M@PANI systems and the values are more negative indicating that the active site is positioned and will not easily be regenerated for further reaction. Hence, metals other than Ni@PANI were included in the electrochemical reduction of CO_2. The calculated Gibbs free energy profiles of CO_2 to HCOOH conversion through formate and carboxylate pathways are presented in Fig. 10 and 11 respectively.

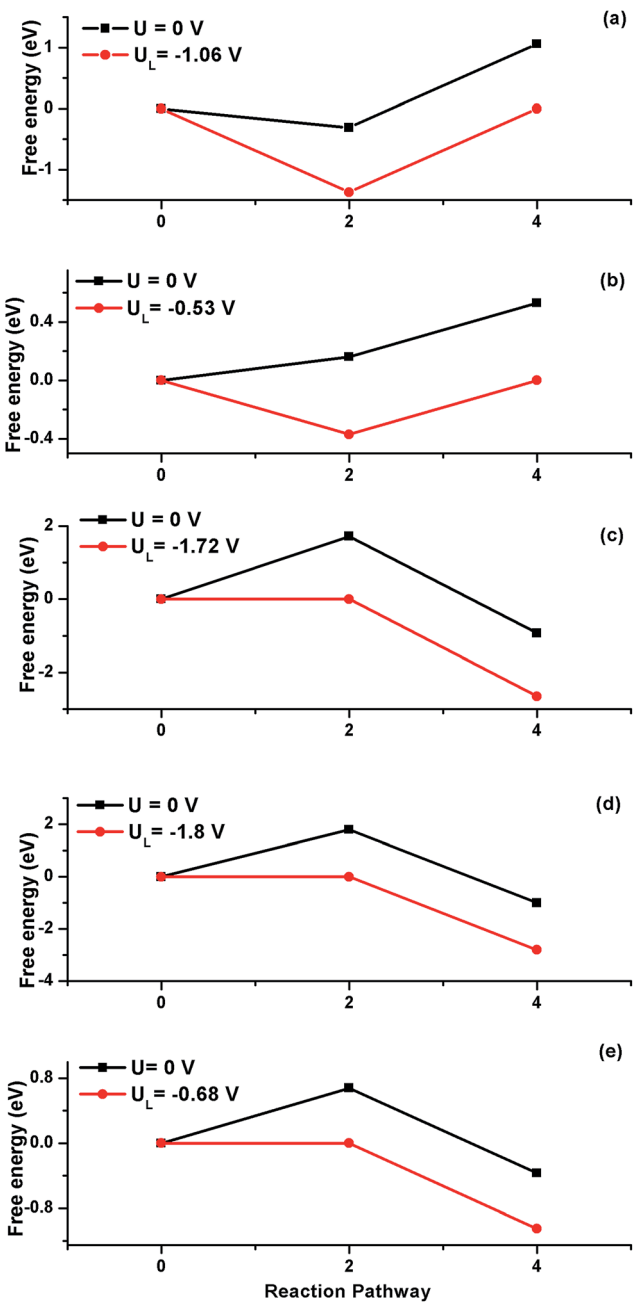

Fig. 11 Calculated Gibbs free energy profile without (U-black lines), and with applied potential (U_L-red lines) for CO_2 electroreduction to HCOOH through carboxylate pathway on M@PANI where M = (a) Pd, (b) Pt, (c) Cu, (d) Ag, and (e) Au.

Reactions of $CO_{2(g)} + H^+ + e^- \rightarrow HCOO^-$ and $HCOO^- + H^+ + e^- \rightarrow HCOOH$, on M@PANI have an uphill step with an energy barrier (Fig. 10) of 0.88 eV, 0.85 eV, 0.48 eV, 0.71 eV and 0.58 eV for the metals of Pd, Pt, Cu, Ag and Au respectively at an applied potential of 0 V. It is interesting to note that the energy barrier is independent of metals which reveal that the reaction step in Pd, Pt and Cu is HCOO to HCOOH and, in Ag and Au, CO_2 to COO^- are the rate determining steps in CO_2 to HCOOH transformation.

In carboxylate reaction path, the calculated energy barriers (Fig. 11) for the step $CO_{2(g)} + H^+ + e^- \rightarrow COOH$ are 1.06 eV, 0.53 eV, 1.72 eV, 1.80 eV and 0.68 eV respectively for Pd, Pt, Cu, Ag and Au on PANI. For Pd and Pt, COOH to HCOOH and, in Cu, Ag and Au, CO_2 to COOH are the rate determining steps respectively in the reduction of CO_2 to HCOOH.

A comparison of the energy barrier values suggests that metal on PANI plays an important role in controlling the rate determining step and also the reaction pathway. For Pd@PANI, Ag@PANI and Au@PANI, energy barrier for the formate path way is less compared to that of the carboxylate route. In contrast to this for Pt@PANI, the carboxylate route has lower barrier. The reaction barrier can be moved further downhill by means of applying extra potential (limiting potential). The required limiting potentials correspond to the same barrier value with negative sign. By applying this limiting potential, the energy barrier is nullified and the reaction proceeds in the forward direction. The order of over potential to be applied on M@PANI for CO_2 to HCOOH transformation is found to be: Cu < Au < Ag < Pt < Pd. This observed activity is mainly controlled by the HOMO–LUMO gap of the M@PANI systems. The HOMO–LUMO gap of the M@PANI follows in the order of Cu > Au > Ag > Pt > Pd. This result indicates that higher the HOMO–LUMO gap favour in lowering of the over potentials.

Conclusion

In the present work, we have explored the activation and transformation of CO_2 to HCOOH on the catalytic metal cluster sites anchored on polyaniline support by employing DFT/B3LYP level of theory. Binding energy reveals that anchoring of metal cluster on PANI is thermodynamically feasible. The frontier molecular orbital analysis of the catalyst predicts the order of HOMO–LUMO gaps for different metal atoms to be Cu > Au > Ag > Pt > Pd, which reveals the order of reactivity as Cu < Au < Ag < Pt < Pd. Data on PDOS reveal that M@PANI retains the conducting behaviour of and involvement of d orbitals too. Calculation of vibrational frequencies of the adsorbed configurations indicates their stability due to the presence in energy minima. Geometry optimisation and electrochemical reduction studies for the carboxylate and formate pathway revealed that the formate pathway is favoured on M@PANI. Among the different metals, Cu appears to be most preceded one.

Acknowledgements

We acknowledge Department of Science and Technology (DST), India, for setting up the National Centre for Catalysis Research (NCCR) at India Institute of Technology Madras (IITM). The authors also acknowledge the High Performance Computing Environment (HPCE), IITM for providing computational facilities. The author, R. S, is thankful to Council for Scientific and Industrial Research (CSIR) for providing financial support vide., Ref. No. 08/117(0001)-2013-EMR-I.

References

1 O. Inganäs and V. Sundström, *Ambio*, 2015, **45**, 15–23.
2 D. R. Kauffman, J. Thakkar, R. Siva, C. Matranga, P. R. Ohodnicki, C. Zeng and R. Jin, *ACS Appl. Mater. Interfaces*, 2015, **7**, 15626–15632.
3 S. E. Hosseini and M. A. Wahid, *Renewable Sustainable Energy Rev.*, 2016, **57**, 850–866.
4 W.-H. Wang, Y. Himeda, J. T. Muckerman, G. F. Manbeck and E. Fujita, *Chem. Rev.*, 2015, **115**, 12936–12973.
5 J. Klankermayer and W. Leitner, *Philos. Trans. R. Soc., A*, 2016, **374**, 1–8.
6 G. Centi, E. A. Quadrelli and S. Perathoner, *Energy Environ. Sci.*, 2013, **6**, 1711–1731.
7 S. Moret, P. J. Dyson and G. Laurenczy, *Nat. Commun.*, 2014, **5**, 1–7.
8 X. Liu, S. Li, Y. Liu and Y. Cao, *Chin. J. Catal.*, 2015, **36**, 1461–1475.
9 W. Leitner, *Angew. Chem., Int. Ed. Engl.*, 1995, **34**, 2207–2221.
10 H. Jeon, B. Jeong, J. Joo and J. Lee, *Electrocatalysis*, 2014, **6**, 20–32.
11 N. V. Rees and R. G. Compton, *J. Solid State Electrochem.*, 2011, **15**, 2095–2100.
12 K. Jiang, H.-X. Zhang, S. Zou and W.-B. Cai, *Phys. Chem. Chem. Phys.*, 2014, **16**, 20360–20376.
13 A. K. Singh, S. Singh and A. Kumar, *Catal. Sci. Technol.*, 2016, **6**, 12–40.
14 O. R. Luca and A. Q. Fenwick, *J. Photochem. Photobiol., B*, 2015, **152**, 26–42.
15 I. Ganesh, *Renewable Sustainable Energy Rev.*, 2016, **59**, 1269–1297.
16 A. J. Martin, G. O. Larrazabal and J. Perez-Ramirez, *Green Chem.*, 2015, **17**, 5114–5130.
17 P. Kang, Z. Chen, M. Brookhart and T. J. Meyer, *Top. Catal.*, 2014, **58**, 30–45.
18 R. J. Lim, M. Xie, M. A. Sk, J.-M. Lee, A. Fisher, X. Wang and K. H. Lim, *Catal. Today*, 2014, **233**, 169–180.
19 J.-P. Jones, G. K. S. Prakash and G. A. Olah, *Isr. J. Chem.*, 2014, **54**, 1451–1466.
20 F. A. Viva, *Adv. Chem. Lett.*, 2013, **1**, 225–236.
21 R. P. S. Chaplin and A. A. Wragg, *J. Appl. Electrochem.*, 2003, **33**, 1107–1123.
22 S. Lee, H. Ju, R. Machunda, S. Uhm, J. K. Lee, H. J. Lee and J. Lee, *J. Mater. Chem. A*, 2015, **3**, 3029–3034.
23 R. Kortlever, C. Balemans, Y. Kwon and M. T. M. Koper, *Catal. Today*, 2015, **244**, 58–62.
24 Y. Fu, Y. Liu, Y. Li, J. Qiao and X.-D. Zhou, *ECS Trans.*, 2015, **66**, 53–59.
25 S. Y. Choi, S. K. Jeong, H. J. Kim, I.-H. Baek and K. T. Park, *ACS Sustainable Chem. Eng.*, 2016, **4**, 1311–1318.
26 R. Kortlever, I. Peters, S. Koper and M. T. M. Koper, *ACS Catal.*, 2015, **5**, 3916–3923.
27 N. Elgrishi, S. Griveau, M. B. Chambers, F. Bedioui and M. Fontecave, *Chem. Commun.*, 2015, **51**, 2995–2998.
28 D. H. Won, J. Chung, S. H. Park, E.-H. Kim and S. I. Woo, *J. Mater. Chem. A*, 2015, **3**, 1089–1095.
29 S. Zhang, P. Kang, S. Ubnoske, M. K. Brennaman, N. Song, R. L. House, J. T. Glass and T. J. Meyer, *J. Am. Chem. Soc.*, 2014, **136**, 7845–7848.
30 D. Li, J. Huang and R. B. Kaner, *Acc. Chem. Res.*, 2009, **42**, 135–145.
31 H. Bejbouj, L. Vignau, J. L. Miane, T. Olinga, G. Wantz, A. Mouhsen, E. M. Oualim and M. Harmouchi, *Mater. Sci. Eng., B*, 2010, **166**, 185–189.
32 Y. F. Huang, C. S. Chang and C. W. Lin, *Int. J. Hydrogen Energy*, 2012, **37**, 11975–11983.
33 L. J. Sun and X. X. Liu, *Eur. Polym. J.*, 2008, **44**, 219–224.
34 S. Mondal, U. Rana and S. Malik, *Chem. Commun.*, 2015, **51**, 12365–12368.
35 T. Lindfors and A. Ivaska, *Anal. Chem.*, 2004, **76**, 4387–4394.
36 Y. Xia and H. Zhu, *Soft Matter*, 2011, **7**, 9388–9393.
37 J. R. Santos Jr, L. H. C. Mattoso and A. J. Motheo, *Electrochim. Acta*, 1998, **43**, 309–313.
38 A. Thota, R. Arukula, R. Narayan, C. R. K. Rao and K. V. S. N. Raju, *RSC Adv.*, 2015, **5**, 106523–106535.
39 Z. Qiang, G. Liang, A. Gu and L. Yuan, *Mater. Lett.*, 2014, **115**, 159–161.
40 X. Feng, C. Mao, G. Yang, W. Hou and J.-J. Zhu, *Langmuir*, 2006, **22**, 4384–4389.
41 H. H. Zhou, S. Q. Jiao, J. H. Chen, W. Z. Wei and Y. F. Kuang, *J. Appl. Electrochem.*, 2004, **34**, 455–459.
42 R. M. Mohamed and E. S. Aazam, *Appl. Catal., A*, 2014, **480**, 100–107.
43 M. H. Beyzavi, R. C. Klet, S. Tussupbayev, J. Borycz, N. A. Vermeulen, C. J. Cramer, J. F. Stoddart, J. T. Hupp and O. K. Farha, *J. Am. Chem. Soc.*, 2014, **136**, 15861–15864.
44 Q.-W. Song, W.-Q. Chen, R. Ma, A. Yu, Q.-Y. Li, Y. Chang and L.-N. He, *ChemSusChem*, 2015, **8**, 821–827.
45 K. A. Weerakoon, J. H. Shu, M.-K. Park and B. A. Chin, *ECS J. Solid State Sci. Technol.*, 2012, **1**, Q100–Q105.
46 A. Nirmala Grace and K. Pandian, *Electrochem. Commun.*, 2006, **8**, 1340–1348.
47 T. C. D. Doan, R. Ramaneti, J. Baggerman, J. F. van der Bent, A. T. M. Marcelis, H. D. Tong and C. J. M. van Rijn, *Sens. Actuators, B*, 2012, **168**, 123–130.
48 F. Köleli and T. Röpke, *Appl. Catal., B*, 2006, **62**, 306–310.
49 D. B. Kayan and F. Köleli, *Appl. Catal., B*, 2016, **181**, 88–93.
50 C. Costentin, M. Robert and J.-M. Saveant, *Chem. Soc. Rev.*, 2013, **42**, 2423–2436.
51 T. N. Huan, E. S. Andreiadis, J. Heidkamp, P. Simon, E. Derat, S. Cobo, G. Royal, A. Bergmann, P. Strasser, H. Dau, V. Artero and M. Fontecave, *J. Mater. Chem. A*, 2015, **3**, 3901–3907.

52 W. Lv, J. Zhou, F. Kong, H. Fang and W. Wang, *Int. J. Hydrogen Energy*, 2016, **41**, 1585–1591.
53 J. S. Yoo, R. Christensen, T. Vegge, J. K. Nørskov and F. Studt, *ChemSusChem*, 2016, **9**, 358–363.
54 D. Chowdhury, *J. Phys. Chem. C*, 2011, **115**, 13554–13559.
55 X. L. Dong, X. F. Zhang, H. Huang and F. Zuo, *Appl. Phys. Lett.*, 2008, **92**, 013127.
56 C. Zhao, Z. Yin and J. Wang, *ChemElectroChem*, 2015, **2**, 1974–1982.
57 R. Aydın, H. Ö. Doğan and F. Köleli, *Appl. Catal., B*, 2013, **140–141**, 478–482.
58 P. Paulraj, N. Janaki, S. Sandhya and K. Pandian, *Colloids Surf., A*, 2011, **377**, 28–34.
59 U. Bogdanović, I. Pašti, G. Ćirić-Marjanović, M. Mitrić, S. P. Ahrenkiel and V. Vodnik, *ACS Appl. Mater. Interfaces*, 2015, **7**, 28393–28403.
60 W. Q. Tian, M. Ge, B. R. Sahu, D. Wang, T. Yamada and S. Mashiko, *J. Phys. Chem. A*, 2004, **108**, 3806–3812.
61 S. N. Khanna, M. Beltran and P. Jena, *Phys. Rev. B: Condens. Matter*, 2001, **64**, 235419–235422.
62 S. J. Li, X. Zhou and W. Q. Tian, *J. Phys. Chem. A*, 2012, **116**, 11745–11752.
63 S. Gautam, K. Dharamvir and N. Goel, *Comput. Theor. Chem.*, 2013, **1009**, 8–16.
64 S. Xu, Z. Wang, C. Wang, Z. Wang and Y. Cui, *New J. Chem.*, 2015, **39**, 3105–3108.
65 C. Jia and W. Fan, *Phys. Chem. Chem. Phys.*, 2015, **17**, 30736–30743.
66 E. D. Glendening, A. E. Reed, J. E. Carpenter and F. Weinhold, *NBO Version 3.1*.
67 J. K. Nørskov, J. Rossmeisl, A. Logadottir, L. Lindqvist, J. R. Kitchin, T. Bligaard and H. Jónsson, *J. Phys. Chem. B*, 2004, **108**, 17886–17892.
68 A. A. Peterson, F. Abild-Pedersen, F. Studt, J. Rossmeisl and J. K. Norskov, *Energy Environ. Sci.*, 2010, **3**, 1311–1315.
69 C. Liu, H. He, P. Zapol and L. A. Curtiss, *Phys. Chem. Chem. Phys.*, 2014, **16**, 26584–26599.
70 M. J. Frisch, G. W. Trucks, H. B. Schlegel, G. E. Scuseria, M. A. Robb, J. R. Cheeseman, G. Scalmani, V. Barone, B. Mennucci, G. A. Petersson, H. Nakatsuji, M. Caricato, X. Li, H. P. Hratchian, A. F. Izmaylov, J. Bloino, G. Zheng, J. L. Sonnenberg, M. Hada, M. Ehara, K. Toyota, R. Fukuda, J. Hasegawa, M. Ishida, T. Nakajima, Y. Honda, O. Kitao, H. Nakai, T. Vreven, J. A. Montgomery Jr, J. E. Peralta, F. Ogliaro, M. J. Bearpark, J. Heyd, E. N. Brothers, K. N. Kudin, V. N. Staroverov, R. Kobayashi, J. Normand, K. Raghavachari, A. P. Rendell, J. C. Burant, S. S. Iyengar, J. Tomasi, M. Cossi, N. Rega, N. J. Millam, M. Klene, J. E. Knox, J. B. Cross, V. Bakken, C. Adamo, J. Jaramillo, R. Gomperts, R. E. Stratmann, O. Yazyev, A. J. Austin, R. Cammi, C. Pomelli, J. W. Ochterski, R. L. Martin, K. Morokuma, V. G. Zakrzewski, G. A. Voth, P. Salvador, J. J. Dannenberg, S. Dapprich, A. D. Daniels, Ö. Farkas, J. B. Foresman, J. V. Ortiz, J. Cioslowski and D. J. Fox, *Gaussian Revision C.01*, 2009.
71 N. M. O'Boyle, A. L. Tenderholt and K. M. Langner, *J. Comput. Chem.*, 2008, **29**, 839–845.
72 S. H. Ahn and H. Lee, *Bull. Korean Chem. Soc.*, 2016, **37**, 27–32.
73 S. Nayab, H.-I. Lee and J. H. Jeong, *Acta Crystallogr., Sect. E: Struct. Rep. Online*, 2013, **69**, m238–m239.
74 S.-Y. Lai, T.-W. Lin, Y.-H. Chen, C.-C. Wang, G.-H. Lee, M.-h. Yang, M.-k. Leung and S.-M. Peng, *J. Am. Chem. Soc.*, 1999, **121**, 250–251.
75 Y. Kim and S. K. Kang, *Acta Crystallogr., Sect. E: Struct. Rep. Online*, 2015, **71**, 1058–1060.
76 X. P. Chen, J. K. Jiang, Q. H. Liang, N. Yang, H. Y. Ye, M. Cai, L. Shen, D. G. Yang and T. L. Ren, *Sci. Rep.*, 2015, **5**, 16907.
77 H. Ullah, A.-U.-H. A. Shah, S. Bilal and K. Ayub, *J. Phys. Chem. C*, 2013, **117**, 23701–23711.
78 H. J. Freund and M. W. Roberts, *Surf. Sci. Rep.*, 1996, **25**, 225–273.